

## Growth and electrochromic properties of single-crystal $V_2O_5$ nanorod arrays

Katsunori Takahashi,<sup>a)</sup> Ying Wang, and Guozhong Cao<sup>b)</sup>

*Materials Science and Engineering, University of Washington, Seattle, Washington*

(Received 30 September 2004; accepted 4 December 2004; published online 24 January 2005)

This paper reports a study on the template-based growth and electrochromic properties of single-crystal vanadium pentoxide nanorod arrays by sol electrophoretic deposition. The formation of single-crystal vanadium pentoxide nanorods is attributed to the homoepitaxial aggregation of nanoparticles. Nanorod arrays have demonstrated significantly enhanced electrochromic properties; both the larger change of transmittance intensity and more rapid response upon applying external electric field are attributed to the large surface to volume ratio and improved transport kinetics for electrochemical intercalation. © 2005 American Institute of Physics. [DOI: 10.1063/1.1857087]

Electrochromic materials are those which exhibit a reversible optical change between the transparent state and the colored state upon charging or discharging via electrochemical reactions.<sup>1</sup> Variable transmittance windows (smart windows), display devices, and controlled reflectance mirrors for vehicles are typical applications of this property, and the smart window is currently one of the most dynamic research areas.<sup>2,3</sup> Vanadium pentoxide ( $V_2O_5$ ) with a layered structure,<sup>4</sup> is promising for smart window applications. However, the diffusion coefficient of Li ions in  $V_2O_5$  ( $10^{-12}$ – $10^{-13}$   $cm^2/s$ )<sup>5,6</sup> and the electrical conductivity of  $V_2O_5$  ( $10^{-2}$ – $10^{-3}$   $S/cm$ )<sup>7,8</sup> are both small and, thus the intercalation process is relatively slow. A large surface area and a short diffusion distance are desired to achieve faster intercalation and extraction kinetics.<sup>9,10</sup> One effective way to achieve these properties is the use of one-dimensional nanostructures, such as nanowires, nanorods, and nanotubes. Although various methods have been developed for the formation of nanorods or nanowires,<sup>11</sup> template-based synthesis is one of the most attractive fabrication methods as this approach provides unidirectionally aligned uniformly sized nanorod arrays.<sup>12–16</sup> This letter reports a study on growth of single-crystal  $V_2O_5$  nanorod arrays using electrophoretic deposition combined with template-based methods, and their improved electrochromic properties.

The chemicals for the synthesis of sol were  $V_2O_5$  (Alfa Aesar), 30%  $H_2O_2$  (J. T. Baker), and  $H_2SO_4$  (96.5%, Fisher).  $V_2O_5$  gel was synthesized using a method reported by Fontenot *et al.*,<sup>17</sup> and a 0.005 mol/l  $V_2O_5$  sol for electrophoretic deposition was prepared by redispersing  $V_2O_5$  gel into deionized water.<sup>18</sup>  $V_2O_5$  nanorod arrays have been grown inside polycarbonate templates with the assistance of electric field, and a detailed description of the deposition setup can be found in our early publications.<sup>13</sup> Sol-gel  $V_2O_5$  film was also prepared and studied for comparison purposes. Such prepared sol-gel film is uniform and crackfree with a thickness of  $\sim 1$   $\mu m$ . The resulting  $V_2O_5$  nanorods and films were characterized by x-ray diffraction (XRD), scanning and transmission electron microscopy (SEM/TEM). Optical absorption spectra were carried out in the range of 380 nm to 900 nm using fiber optic spectrometer under a dc voltage of

2.0 V and 3.0 V, with a 1M- $LiClO_4$  solution in propylene carbonate as electrolyte, platinum counter electrode and Ag/AgNO<sub>3</sub> reference electrode. A chronopotentiostat measurement was carried out by a potentiostat/galvanostat.

Figure 1(a) shows a typical SEM image of  $V_2O_5$  nanorod arrays on a tin doped indium oxide (ITO) substrate.  $V_2O_5$  nanorods are arranged almost parallel to one another over a large area, and stand perpendicular to the substrate. The diameters of these nanorods are about 100 nm, which had 50% lateral shrinkage after firing, however there is negligible shrinkage along the axis. Figures 1(b) and 1(d) show a typical TEM image of a  $V_2O_5$  nanorod and selected area electron diffraction pattern, which clearly demonstrated the single-crystalline nature or, at least, well textured nature of the grown nanorods with a [010] growth direction. Figure 1(c) shows a high-resolution TEM image of the single  $V_2O_5$  nanorod, in which lattice fringes are clearly visible. The spacing of the fringes was measured to be 0.208 nm, which

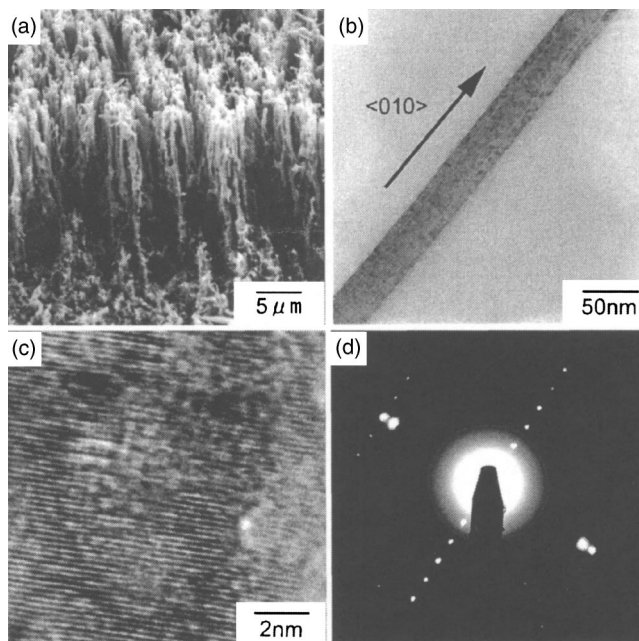


FIG. 1. (a) SEM image of  $V_2O_5$  nanorod arrays on an ITO substrate grown in a 200 nm PC membrane by sol electrophoretic deposition. TEM images of  $V_2O_5$  nanorod (b) and high-resolution image showing the lattice fringes (c), and electron diffraction pattern (d).

<sup>a)</sup>Current address: Steel Research Laboratory, JFE Steel Corporation, Japan.

<sup>b)</sup>Electronic mail: gzcao@u.washington.edu

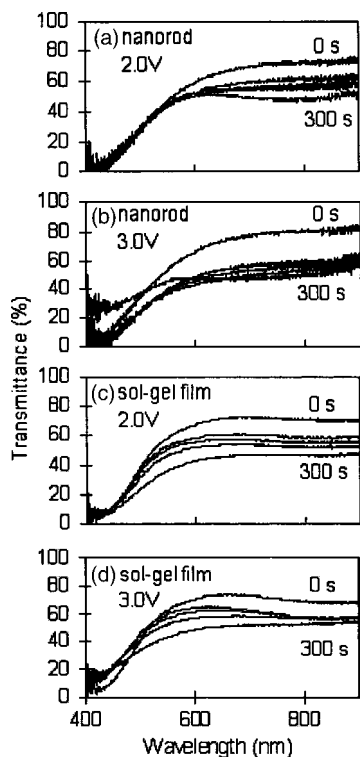


FIG. 2. Transmittance spectra of nanorod arrays under an externally applied electric voltage of (a) 2.0 V and (b) 3.0 V, and of sol-gel derived film under an applied electric voltage of (c) 2.0 V and (d) 3.0 V.

corresponds well with the spacing of (202) planes at 0.204 nm. The formation of single-crystal nanorods can be explained by the homoepitaxial aggregation of crystal nanoparticles. Such homoepitaxial aggregation of crystalline particles is thermodynamically favorable and has been experimentally observed and reported in literature.<sup>19,20</sup> Vanadium oxide nanoparticles in a typical sol are well known to possess ordered crystalline structure easily.<sup>21</sup> When an external electric field results in an oriented migration and enrichment of  $V_2O_5$  nanoparticles at the vicinity of the growth surface, these single-crystal  $V_2O_5$  nanoparticles interact with each other or with the growth surface and start to aggregate. However, initial weak interaction between adjacent nanoparticles or nanoparticle and growth surface permits rotation and migration of such nanoparticles to allow them to find the site and orientation with the lowest interface energy when they finally aggregate. Under favorable experimental conditions, all nanoparticles can aggregate homoepitaxially. The formation of single-crystal  $V_2O_5$  nanorods by sol electrophoretic deposition may well be attributed to such homoepitaxial aggregation of single crystal  $V_2O_5$  nanoparticles. In addition, internal surface of pore channels might promote the orientation of nanocrystals. It is expected that such formed single crystals would have a highly porous microstructure, which undergo significant shrinkage when fired at elevated temperatures.

Figure 2 shows typical optical transmittance spectra of the nanorod arrays and film when applying voltages of 2.0 and 3.0 V. The overall intensity of transmittance spectra of the samples reduces as the time increases. However, such a change is due to a combined contribution of  $V_2O_5$  nanorod and bare ITO substrate, since ITO also changes its transparency by lithium intercalation.<sup>22</sup> So, we calibrated the trans-

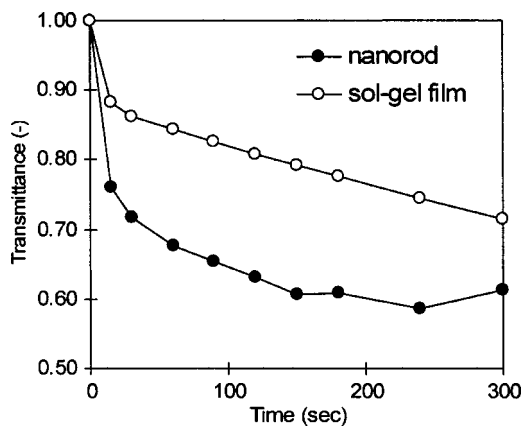


FIG. 3. Transmittance intensity of nanorod arrays and sol-gel films as a function of time subjected to an externally applied electric field.

mittance of  $V_2O_5$  by subtracting ITO transmittance as follows:

$$A_{V_2O_5} \times (100 - I_{(V_2O_5)}) + A_{ITO}(100 - I_{m(ITO)}) \\ + (100 - I_{sub}) = 100 - I_{m(V_2O_5+ITO)}$$

$$I_{C(V_2O_5)} = 100 - \{I_{sub} - I_m - A_{ITO} \\ \times (100 - I_{m(ITO)})\} / A_{V_2O_5}$$

where  $I_{C(V_2O_5)}$  is the calculated transparency of  $V_2O_5$  nanorod array,  $I_{m(V_2O_5+ITO)}$  is the observed transparency of  $V_2O_5$  nanorod array on an ITO substrate at  $t$ (s),  $I_{m(ITO)}$  is the observed transparency of an ITO substrate at  $t$  (sec),  $I_{m(ITO)}$  is the initial transparency of ITO substrate,  $A_{ITO}$  is the area of the bare ITO substrate, and  $A_{V_2O_5}$  is the area covered with  $V_2O_5$  nanorod array.

The calibrated transmittance of  $V_2O_5$  nanorod arrays are shown in Figures 2(a) and 2(b). Transmittance at a wavelength around 700 nm was reduced along with time, while a voltage of 2.0 V was applied, similar results were found in sol-gel derived  $V_2O_5$  film [Fig. 2(c)]. These experimental results also agree very well with the literature.<sup>23,24</sup> Although the general trend of spectrum change is similar in both nanorod arrays and sol-gel film, the responding speed of  $V_2O_5$  nanorod arrays is significantly faster than that of sol-gel derived film. Figure 3 shows the change of transmittance intensity at 700 nm as a function of time when 3.0 V is applied. 30% reduction was achieved in  $\sim 50$  s in nanorod array, however, 300 s were required in sol-gel  $V_2O_5$  film. The transmittance change of nanorods array reached saturation in 3 min, while sol-gel derived film was not saturated in 5 min. Extrapolation from the data in Fig. 3 suggests that sol-gel film would require at least 10 min to reach the same saturation, i.e., sol-gel film has a three times slower responding speed than the nanorod array.

The differences in electrochromic properties are attributed to the differences in microstructure and nanostructures.  $V_2O_5$  nanorods are single crystal with  $V_2O_5$  layers parallel to the nanorod growth direction. Such a structure is extremely favorable to  $Li^+$  intercalation and extraction, since the redox reactions occur on the surface and the solid-state diffusion distance is very small,  $\sim 50$  nm, one-half of the diameter of nanorods. In addition, such a well-aligned structure would also enhance the  $Li^+$  diffusion through the solvent. Sol-gel

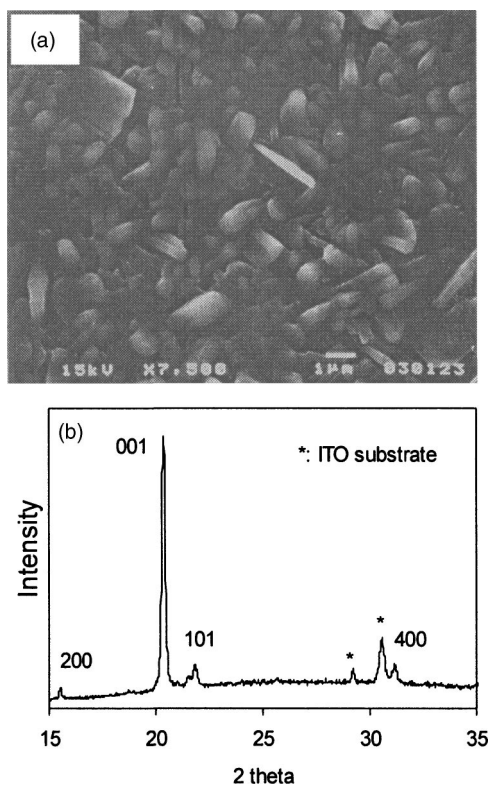


FIG. 4. (a) SEM image and (b) XRD spectrum of  $V_2O_5$  film on an ITO substrate.

$V_2O_5$  films are polycrystalline and consist of micron-sized platelets with [001] perpendicular to the substrate surface as shown in Figs. 4(a) and 4(b). Therefore, the  $Li^+$  intercalation and extraction processes would comprise of  $Li^+$  diffusion along grain boundaries, redox reactions at the surface of individual grains, and diffusion inside individual grains. This difference in microstructure and nanostructure has also been reflected in the electrochemical property characterization as described below.

Figure 5 shows the comparison between the current density and  $Li^+$  insertion capacity of nanorod arrays and sol-gel films. Capacities of both nanorod arrays and film are the

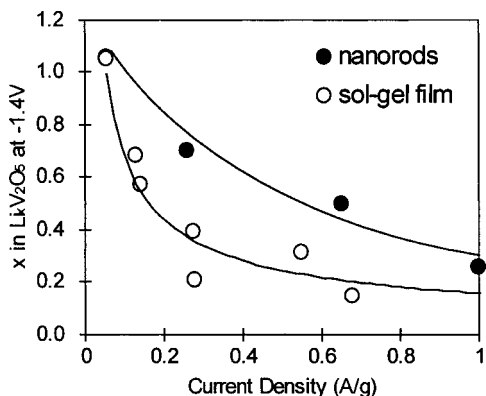


FIG. 5. Plot of discharge capacity versus current density for both  $V_2O_5$  nanorod arrays (solid dots) and sol-gel derived films (empty circles).

same when small current density is applied, since the intercalation process proceeds close to thermodynamic equilibrium. However, when larger current densities are applied, nanorod arrays can intercalate much higher amounts of  $Li^+$ ; for example, 2.5 times higher  $Li^+$  can be intercalated into nanorod arrays than sol-gel derived film with a given current density. The results in Fig. 5 unambiguously corroborate and explain the electrochromic properties presented in Fig. 3.

In summary, single-crystal  $V_2O_5$  nanorods were grown by sol electrophoretic deposition with a length of about  $10 \mu m$  and a diameter of about  $100 nm$ , and nearly unidirectional alignment over a large area, and they have single-crystalline structure with [010] growth axis. The formation of single-crystal nanorods was attributed to homoepitaxial aggregation of single-crystal nanoparticles. Both the extent and speed of change in transmittance intensity of nanorod array are significantly faster than those of sol-gel derived film, corroborating with an enhanced electrochemical intercalation process in nanorod arrays due to large surface area for surface redox reaction and short and easy diffusion path for mass and charge transport.

One of the authors (Y.W.) would like to acknowledge financial support from the Ford Motor Company Fellowship.

- <sup>1</sup>R. D. Rauh, *Electrochim. Acta* **44**, 3165 (1999).
- <sup>2</sup>D. R. Rosseinsky and R. J. Motimer, *Adv. Mater. (Weinheim, Ger.)* **13**, 783 (2001).
- <sup>3</sup>N. M. Rowley and R. J. Mortimer, *Sci. Prog.* **85**, 243 (2002).
- <sup>4</sup>*Chemical Physics of Intercalation*, edited by A. P. Legrand and S. Flanodis, NATO Ser. B172 (Plenum, New York, 1987).
- <sup>5</sup>E. Portiron, A. L. Salle, A. Varbaere, Y. Piffard, and D. Guyomard, *Electrochim. Acta* **45**, 197 (1999).
- <sup>6</sup>F. Lantelme, A. Mantoux, H. Groult, and D. Lincot, *J. Electrochem. Soc.* **150**, A1202 (2003).
- <sup>7</sup>F. Coustier, J. Hill, B. B. Owens, S. Passerini, and W. H. Smyrl, *J. Electrochem. Soc.* **146**, 1355 (1999).
- <sup>8</sup>J. Livage, *Chem. Mater.* **3**, 578 (1991).
- <sup>9</sup>T. Watanabe, Y. Ikeda, T. Ono, M. Hibino, M. Hosoda, K. Sakai, and T. Kudo, *Solid State Ionics* **151**, 313 (2002).
- <sup>10</sup>M. J. Parent, S. Passerini, B. B. Owens, and W. H. Smyrl, *Electrochim. Acta* **44**, 2209 (1999).
- <sup>11</sup>G. Z. Cao, *Nanostructures and Nanomaterials: Synthesis, Properties, and Applications* (Imperial College Press, London, 2004).
- <sup>12</sup>P. Sarkar and P. S. Nicholson, *J. Am. Ceram. Soc.* **79**, 1987 (1996).
- <sup>13</sup>S. J. Limmer, S. Seraji, M. J. Forbess, Y. Wu, T. P. Chou, C. Nguyen, and G. Z. Cao, *Adv. Mater. (Weinheim, Ger.)* **13**, 1269 (2001).
- <sup>14</sup>S. J. Limmer, S. Seraji, M. J. Forbess, Y. Wu, T. P. Chou, C. Nguyen, and G. Z. Cao, *Adv. Funct. Mater.* **12**, 59 (2002).
- <sup>15</sup>K. Takahashi, S. J. Limmer, and G. Z. Cao, *Proc. SPIE* **5224**, 33 (2004).
- <sup>16</sup>K. Takahashi, S. J. Limmer, Y. Wang, and G. Z. Cao, *J. Phys. Chem. B* **108**, 9795 (2004).
- <sup>17</sup>J. Fontenot, J. W. Wiench, M. Pruski, and G. L. Schrader, *J. Phys. Chem. B* **B104**, 11622 (2000).
- <sup>18</sup>K. Takahashi, S. J. Limmer, Y. Wang, and G. Z. Cao, *Jpn. J. Appl. Phys.* (to be published).
- <sup>19</sup>R. L. Penn and J. F. Banfield, *Geochim. Cosmochim. Acta* **63**, 1549 (1999).
- <sup>20</sup>C. M. Chun, A. Navrotsky, and I. A. Aksay, *Proc. Microscopy and Microanalysis* (Jones and Begell, New York, 1995), p. 188.
- <sup>21</sup>J. Livage, *Coord. Chem. Rev.* **178**, 999 (1998).
- <sup>22</sup>Z. Wang and X. Hu, *Thin Solid Films* **392**, 22 (2001).
- <sup>23</sup>H. Watanabe, K. Itoh, and O. Matsumoto, *Thin Solid Films* **386**, 281 (2001).
- <sup>24</sup>E. E. Chain, *Appl. Opt.* **30**, 2782 (1991).